AMSE JOURNALS-AMSE IIETA publication-2017-Series: Advances C; Vol. 72; N°2; pp 140-155
Submitted Mar. 23, 2017; Revised May 09, 2017; Accepted Jun. 12, 2017

Clutch Displacement Servo Control in Gear-Shifting Process of Electric Vehicles Based on Two-speed DCT

* Xi Liu, ** Ren He, *** Yongdao Song

* School of Automotive & Traffic Engineering, Jiangsu University, Zhenjiang 212013, China (xiliu@ujs.edu.cn)
** School of Automotive & Traffic Engineering, Jiangsu University, Zhenjiang 212013, China
*** Shanghai Automobile Gear Works, Jiading 201807, China

Abstract

Two-speed dual-clutch transmission (DCT) is an ideal transmission mode for electric vehicles. After analysing the power transmission system of electric vehicles installed with two-speed DCT, this paper constructs the lever spring model of dual dry clutch, torque transmission model of friction plate, and clutch actuator model, and utilizes the models to identify the relationship between torque transmission and release bearing displacement of the clutch. According to the nonlinear features of the clutch, the author proposed the strategy of clutch displacement servo control under the inspiration of single-neuron adaptive PID compensation, which improves clutch control accuracy by intelligent compensation based on mathematical model control. Finally, an actual vehicle test was carried out to verify the effectiveness of the proposed strategy. Suffice it to say that the study provides a reference for the control of electric vehicle transmission system.

Key words

Electric vehicles, Dual-clutch transmission (DCT), Proportional flow control valve, Single-neuron adaptive PID control.

1. Introduction

Amidst the growing oil shortage around the world, the automotive industry has started a global technological reform of automotive power system, seeking to overcome the environmental

unfriendliness of traditional fuel vehicles [1]. Free from oil consumption or exhaust discharge, electric vehicles have become a research hotspot in the field of new energy vehicles. As the name implies, an electric vehicle is driven by the electric energy stored in batteries [2-4]. Theoretically, the electric vehicle requires no transmission, for the traction motor, featuring a wide speed range and a large driving torque, can be driven from zero speed under load [5,6]. In practice, however, it is too complex and costly to adopt a reducer with fixed speed ratio. With such a reducer, the traction motor has to increase the instantaneous torque in the constant torque area, speed up the rotation in the constant power area, and even realize high torque under low speed [7,8]. What is worse, more operating points of the traction motor will fall in the low-speed heavy-load area and high-speed low-load area [9], impeding the economic efficiency of energy consumption.

To solve the above problems of fixed speed ratio transmission, designers often resort to the multi-shift transmission system in the development of electric vehicles. Despite a 5~12% decline in the overall energy consumption, the multi-shift gearbox pushes up the structural complexity and cost control of the transmission system of electric vehicles [10, 11]. Ranging from single-speed transmission, dual-speed transmission, three-speed transmission to continuously variable transmission (CVT), a variety of transmissions have been adopted in the existing all-electric vehicle models. Through experimental comparisons, it is concluded that the two-speed transmission is the most suitable option for all-electric vehicles [12]. The transmission should be further improved by installing two separate clutches for odd and even gear sets. The dual-clutch transmission (DCT) both retains the upsides of the traditional manual transmission (e.g. simple structure, high mechanical efficiency), and realizes sound power performance and cost efficiency with no power interruption in the gear-shifting process. Much research has been done on two-speed DCT in electric vehicles at home and aboard, especially in the aspects of system features, structural optimization, gear shifting pattern, and interaction torque control [13-16]. Nevertheless, little attention has been paid to the clutch control in the gear shifting process.

2. Two-Speed DCT System of Electric Vehicles

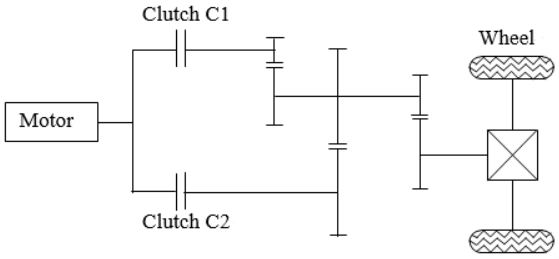

Fig.1. Working principle of electric vehicle

In this research, the power transmission system of electric vehicles mainly consists of a traction motor and a two-speed dry DCT (Figure 1). The traction motor is a permanent magnet brushless DC motor. The DCT is specially designed for electric vehicles, involving two concentric hydraulic dry clutches, each of which is connected to an input shaft. The gears of the solid inner shaft and the hollow outer shaft are respectively engaged with driven gears of the first gear (low speed) and the second gear (high speed). The power transmission system is synchronizer-free, simple in structure and light in weight.

Owing to the low speed and high torque of the permanent magnet brushless DC motor, it is possible to start the vehicle through direct control of the traction motor. Before the starting the vehicle, the first-shift clutch C1 is engaged and the second-shift clutch C2 is separated. When the vehicle starts, C1 is kept in the engaged state and C2 is held in the separated state. In the upshift process, C1 is gradually separated and C2 is gradually separated after detecting the shift point, completing the shift from the current gear to the target gear. When C1 is completely separated and C2 is fully engaged, the first gear is upgraded to second gear. The downshift process is conducted in a similar manner. Without any gear engagement or downshift, the two-speed DCT shortens the gear-shifting time, supplies uninterrupted power, and thus improves the shift comfort and power performance of electric vehicles.

3. Dry Clutches and Proportional Flow Control Valve

As a key component of the DCT, the dry clutches are responsible for torque transmission in the vehicle's power transmission system. In the gear shifting process, the shift quality is positively correlated with the proximity between the actual and the target torques. Hence, it is necessary to analyse the features of the dry clutches and their core component: the proportional flow control valve. Such features are of great importance to achieving the precise clutch control in the gear shifting process.

3.1 Features of Dry Clutches

The dual-clutch in this paper consists of two normally-open dry clutches that operate independently from each other (Figure 2). The two clutches are stacked axially with the input connected to the traction motor. The two clutch plates are respectively linked with the first and second input shafts. The compaction force on the clutch plates is supplied by the lever spring. If the small end of the lever spring is in the complete separation state or under a small force, the

clutches are separated and do not transmit torque; Under the increasing force from the release bearing, the small end of the lever spring is subject to a continuously growing displacement, resulting in greater compaction force on the clutch plates. In short, one can adjust the torque transmitted by the dry clutches through controlling the release bearing displacement, and thereby realize the engagement and separation of the clutches.

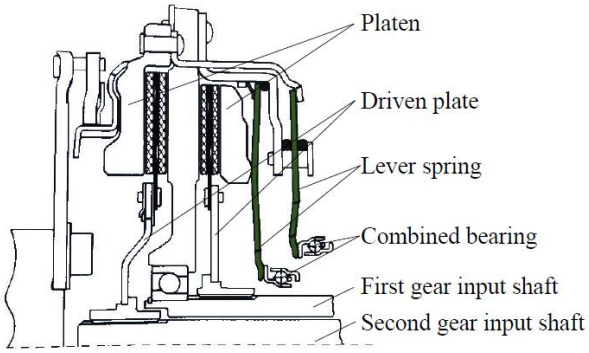

Fig.2. Structure scheme of dry dual clutch

Whereas the two dry clutches have exactly the same structure, clutch C1 was selected as the object of this research. As shown in Figure 3, there are three operating states of the lever spring of clutch C1: the complete separation state, the intermediate state and the complete engagement state.

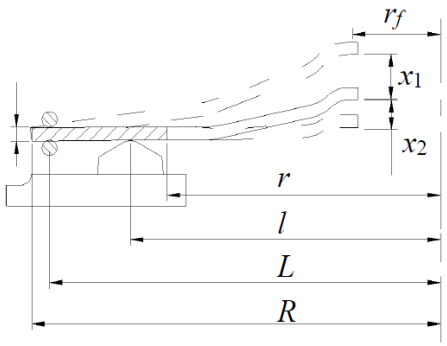

Fig.3. Schematic diagram of lever spring

In the complete separation state, the clutch is completely separated; in the intermediate state, the small end of the lever spring is deformed under the action of the release bearing, resulting in displacement, but the clutch does not transmit torque because the clutch plate and the friction plate are not pressed; in the complete engagement state, the lever spring starts applying pressure on the friction plate through the clutch plate, forcing the clutch to transmit torque.

In the intermediate state, assuming that the lever spring does not deform under the release bearing, and that its meridional cross section rotates around the center point of central cone, the relationship between the force on the lever spring and the small end displacement can be described by the Almen-Laszlo formula. If the displacement of the lever spring-clutch plate in the contact area is denoted as x, then the force applied by the release bearing on the small end of the lever spring can be expressed as:

$$F_1 = \frac{\pi E h x}{6(1-\mu^2)} \frac{\ln(R/r)}{(L-r_f)^2} \left[(H - x\frac{R-r}{L-r_f})(H - \frac{x}{2}\frac{R-r}{L-r_f}) + h^2 \right] \tag{1}$$

where E is the elastic modulus; h is the steel plate thickness of the lever spring; μ is Poisson's ratio; R is the large radius of the disc spring in the complete separation state; r is the small radius of the disc spring in the complete separation state; L is the radius of the support ring; r_f is the radius of the contact area between the release bearing and the small end of lever spring; H is the inner cone height of the disc spring in the complete separation state.

In the complete engagement state, the relationship between the small end displacement x2 and the force applied by the release bearing F2 can be obtained by the cantilever beam mechanics:

$$x_2 = \frac{6F_2 r_f^{\ 2}}{\pi E h^3} (\frac{A_1}{\beta_1} + \frac{A_2}{\beta_2}) \tag{2}$$

$$A_1 = \frac{1}{2}(\frac{r_e^{\ 2}}{r_f^{\ 2}} - 1) - 2(\frac{r_e}{r_f} - 1) + \ln\frac{r_e}{r_f} \tag{3}$$

$$A_2 = \frac{1}{2}(\frac{r^2}{r_f^{\ 2}} - \frac{r_e^{\ 2}}{r_f^{\ 2}}) - 2(\frac{r}{r_f} - \frac{r_e}{r_f}) + \ln\frac{r}{r_e} \tag{4}$$

$$\beta_1 = 1 - \frac{n\delta_1}{\pi(r_e + r_f)} \tag{5}$$

$$\beta_2 = 1 - \frac{n\delta_2}{\pi(r_e + r)} \tag{6}$$

Under the force F_2, the total small end displacement x of the lever spring is:

$$x = x_1 + x_2 \tag{7}$$

Then, the pressing force P of the clutch plate and the force F_2 applied by the release bearing follows the relationship below:

$$P = \frac{L - r_f}{L - l}(F_2 - F_1(x_1)) \tag{8}$$

where l is the radius of loading point of the clutch plate; $F_1(x_1)$ is the force applied on the small end to remove the empty stroke x_1 of the lever spring.

Based on the above formula, it is possible to ascertain the relationship between the pressing force P and the displacement x:

$$P = \begin{cases} 0 & x \le x_1 \\ \dfrac{L - r_f}{L - l}(F_2(x - x_1) - F_1(x_1)) & x > x_1 \end{cases} \tag{9}$$

In the intermediate state, the transmission torque mainly depends on the pressing force and the friction coefficient. The relationship between the transmission torque of the clutch and Z friction surfaces can be expressed as:

$$T_c = Z\mu_c P \frac{2(R_c^{\,3} - r_c^{\,3})}{3(R_c^{\,2} - r_c^{\,2})} \tag{10}$$

where T_c is the transmission torque of clutch; Z is the number of friction surfaces of the clutch; μ_c is coefficient of sliding friction; R_c is the outer diameter of the friction plate; r_c is the inner diameter of the friction plate.

Considering the complete separation state, intermediate state, and complete engagement state, the transmission torque of the dry clutch is:

$$T_c = \begin{cases} 0 & \text{complete separation} \\ sign(\omega_m - \omega_c) Z \mu_c P \dfrac{2(R_c^{\,3} - r_c^{\,3})}{3(R_c^{\,2} - r_c^{\,2})} & \text{partial engagement} \\ T_m & \text{complete engagement} \end{cases} \tag{11}$$

$$sign(\omega_m - \omega_c) = \begin{cases} 1 & \omega_m - \omega_c > 0 \\ -1 & \omega_m - \omega_c < 0 \end{cases} \tag{12}$$

where T_c is the transmission torque of clutch; ω_m is the speed of the traction motor; ω_c is the speed of clutch driven part; T_m is the torque of the traction motor.

3.2 Features of proportional flow control valve

In the two-speed DCT, the release bearing displacement is created as the clutch rod is pushed by the cylinder piston of the clutch; the movement of the piston, however is controlled by the actuator via a proportional flow control valve. The following equation depicts the relationship between the outlet speed of the proportional flow control valve and the speed of clutch cylinder piston:

$$Q_c = 60\pi(\frac{d_p}{2})^2 v_p \tag{13}$$

where Q_c is the outlet speed of the proportional flow control valve; d_p and v_p are the diameter and speed of the clutch cylinder piston, respectively. The v_p is transformed into the speed of the release bearing via the connecting rod, and the displacement of the release bearing can be obtained after the engagement. In other words, the relationship between the outlet speed and the release bearing displacement can be obtained through the feature analysis of the proportional flow control valve.

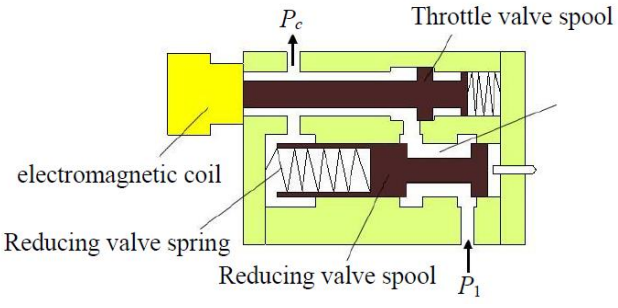

Fig.4. Principle diagram of proportional flow valve

Figure 4 shows the structure of the proportional flow control valve. Since the outlet of the throttle valve is connected to the feedback end of the reducing valve, the fluctuating feedbacks resulted from load variation will bring changes to the throttle valve inlet pressure P2, but will not affect the throttle valve outlet pressure Pc. Therefore, the outlet speed only relies on the opening degree of the throttle valve, making it possible to achieve the flow control by adjusting the proportion of electromagnetic current.

If the spool displacement of the reducing valve is denoted as xr and the spool position at the fully open state is set to 0, and if the spool displacement of the throttle valve is denoted as xt and the spool position at the fully closed state is set to 0, then the spool is subject to the following forces in the axial direction:

(1) When the coil is charged with electricity, the proportion of electromagnetic current in the proportional flow control valve is under the electromagnetic force below:

$$F_e = \frac{N^2 I^2 \mu_0}{2K_f{}^2 \delta^2} S \tag{14}$$

Where F_e is the outlet of proportional flow control valve; N is the number of turns per coil; I is the current; K_f is the leakage coefficient; μ_0 is the vacuum permeability; S is the cross-sectional area of the electromagnetic circuit; δ is the air- gap length.

(2) Since both the reducing valve and throttle valve have a spring, the spring force of the spool obeys the Hooke's law:

$$F_{kr} = F_{kr0} + K_r x_r \tag{15}$$

$$F_{kt} = F_{kt0} + K_t x_t \tag{16}$$

where F_{kr} and F_{kt} are the spring forces of the reducing valve and the throttle valve, respectively; K_r and K_t are the spring stiffness of the reducing valve and the throttle valve, respectively; F_{kr0} and F_{kt0} are the spring preloads of the reducing valve and the throttle valve, respectively.

(3) The inertial forces on the moving valve pool can be expressed by Newton's second law of motion:

$$F_{ar} = m_r \ddot{x}_r \tag{17}$$

$$F_{at} = m_t \ddot{x}_t \tag{18}$$

Where F_{ar} and F_{at} are the inertial forces of the reducing valve and the throttle valve, respectively; m_r and m_t are the masses of the reducing valve and the throttle valve, respectively.

(4) The changing flow direction and rate of the working fluid in the valve chamber will cause changes in momentum, applying additional axial steady flow force and transient flow force on the spool:

$$F_{sr} = (2C_{qr}C_{vr}W_r \cos\phi)(H_r - x_r)(P_1 - P_2) \tag{19}$$

$$F_{st} = (2C_{qt}C_{vt}W_t \cos\phi)x_t(P_2 - P_c) \tag{20}$$

Where F_{sr} and F_{st} are the axial steady flow forces of the reducing valve and the throttle valve, respectively; C_{qr} and C_{qt} are the flow coefficients of the reducing valve and the throttle valve, respectively; C_{vr} and C_{vt} are the speed coefficients of the reducing valve and the throttle valve, respectively; W_r and W_t is the flow area gradients of the reducing valve and the throttle valve, respectively; ϕ is the jet angle; H_r is the displacement at the fully open state of the reducing valve spool.

$$F_{ir} = -C_{qr}W_r l_r \sqrt{2\rho(P_1 - P_2)}\dot{x}_r \tag{21}$$

$$F_{it} = -C_{qt}W_t l_t \sqrt{2\rho(P_2 - P_c)}\dot{x}_t \tag{22}$$

Where F_{ir} and F_{it} are the axial transient flow forces of the reducing valve and the throttle valve, respectively; l_r and l_t are the valve chamber lengths of the reducing valve and the throttle valve, respectively; ρ is the working fluid density.

(5) The reducing valve spool and the throttle valve spool also suffer from rightward hydraulic pressures:

$$F_{hr} = \frac{1}{4}\pi P_c D_r^{\ 2} \tag{23}$$

$$F_{ht} = \frac{1}{4}\pi P_c (D_t^{\ 2} - d_t^{\ 2}) \tag{24}$$

Where F_{hr} and F_{ht} are the hydraulic pressures of the reducing valve and the throttle valve, respectively; D_r and D_t are the outer diameters of the reducing valve and the throttle valve, respectively; d_t is the inner diameter of the throttle valve spool.

Through the above force analysis, it is possible to obtain the force equilibrium-equation of proportional flow control valve spool:

$$F_e + F_{ht} = F_{kt} + F_{at} + F_{st} + F_{it} \tag{25}$$

$$F_{ar} + F_{hr} = F_{kr} + F_{sr} + F_{ir} \tag{26}$$

The flow balance equation of proportional flow control valve can be obtained according to the principle of flow balance:

$$Q_i = Q_{rr} + Q_{ro} + Q_{rl} \tag{27}$$

$$Q_{ro} = Q_o + Q_{rf} \tag{28}$$

Where Q_i is the inlet speed of the proportional flow control valve; Q_{rr} is the flow entering the right chamber of the reducing valve; Q_{ro} is the outlet speed of the reducing valve; Q_{rl} is the flow entering the left chamber of the reducing valve; Q_o is the outlet speed of the proportional flow control valve; Q_{rf} is the flow entering the feedback chamber of the reducing valve.

4. Clutch Displacement Servo Control

The lever spring model of dual dry clutch, torque transmission model of friction model, and clutch actuator model lays the basis for current-displacement-torque control. Due to deformation and abrasion in actual practice, there is always a certain deviation between the actual clutch displacement and the theoretical displacement calculated by the mathematical models. Besides, the

accuracy and performance of solenoid valve will deteriorate after long-term use. To minimize the deviation, the single-neuron adaptive PID controller was introduced to the mathematical models.

4.1 Single-neuron adaptive PID controller

Although it is widely utilized thanks to simple structure and convenient adjustment, the traditional PID controller fails to meet the control demand of nonlinear system, as it cannot adjust the control parameters in real time. In this research, the traditional PID controller was improved by the single-neuron controller, which supports self-learning, self-adaptation, and auto adjustment to environmental changes. The two controllers were integrated into a single-neuron adaptive PID controller (Figure 5).

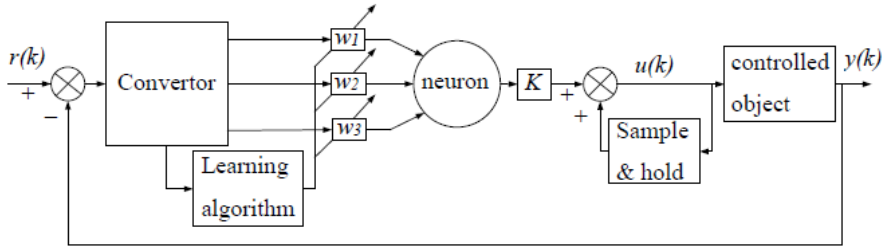

Fig.5. Structure diagram of single neuron adaptive PID controller

The input and output of single-neuron adaptive PID controller are denoted as $r(k)$ and $y(k)$, respectively. The output of the converter is the state quantities $x_1(k)$, $x_2(k)$ and $x_3(k)$ required for neuron learning. The expressions of these state quantities are listed below:

$$\left.\begin{aligned} x_1(k) &= r(k) - y(k) = e(k) \\ x_2(k) &= e(k) - e(k-1) = \Delta e(k) \\ x_3(k) &= e(k) - 2e(k-1) + e(k-2) = \Delta^2 e(k) \end{aligned}\right\} \tag{29}$$

Through correlation search, the neuron generates the control signal $u(k)$:

$$u(k) = u(k-1) + K\sum_{i=1}^{3} w_i(k)x_i(k) \tag{30}$$

where $w_i(k)$ is the weighting coefficient corresponding to $x_i(k)$; K is the neuron scale factor.

The single-neuron adaptive PID controller executes the learning rules in real time and adjusts the weighting factor to achieve the adaptive, self-learning function. Being the most popular learning rule, the Supervised Hebbian Learning enhances the learning capacity of the neuron controller in interaction with the controlled object, and fits in well for real-time control. Hence, the learning rules are adjusted as follows:

$$w_i(k+1) = (1-c)w_i(k) + \eta e(k)u(k)x_i(k) \tag{31}$$

Where c is a constant ($0 \leq c < 1$); η is the learning rate ($\eta > 0$).

For good convergence and robustness, the learning algorithm of single-neuron adaptive PID control was normalized as:

$$\left.\begin{aligned} u(k) &= u(k-1) + K\sum_{i=1}^{3} w_i'(k)x_i(k) \\ w_i'(k) &= w_i(k) / \sum_{i=1}^{3} |w_i(k)| \\ w_1(k+1) &= w_1(k) + \eta_P e(k)u(k)x_1(k) \\ w_2(k+1) &= w_1(k) + \eta_I e(k)u(k)x_2(k) \\ w_1(k+1) &= w_1(k) + \eta_D e(k)u(k)x_3(k) \end{aligned}\right\} \tag{32}$$

Where η_p is the proportional learning rate; η_I is the integral learning rate of integral; η_D is the differential learning rate.

4.2 Clutch Control Based on Single-Neuron Adaptive PID Compensation

To make up for the defect of the mathematic models, the single-neuron adaptive PID controller was applied to clutch displacement servo control. The controller generates the current correction quantity according to the difference between the target displacement and actual displacement of the clutch, aiming to compensate the main current calculated by the mathematical models. With the good adaptive ability, the controller resolves the distortion of the mathematical models after long-term operation, and thereby improves the pressure control accuracy of the clutch. The principles of dry clutch control based on single-neuron adaptive PID are illustrated in Figure 6.

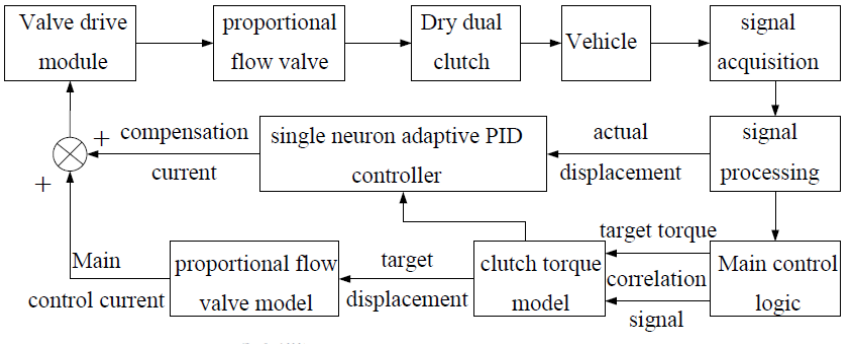

Fig.6. Control schematic diagram of dry dual clutch

It can be seen that the clutch displacement servo control is a compound control measure. Specifically, the model-based control ensures good control effect in the initial phase of neuron learning. On this basis, the single-neuron adaptive PID control makes intelligent compensation to the impreciseness and variation of the models.

5. Clutch Displacement Servo Control

The two-speed DCT was installed to an all-electric vehicle for an actual test on the gear shifting process. The previous models and the single-neuron adaptive PID compensation were taken account of during the test. The test results are depicted in Figure 7.

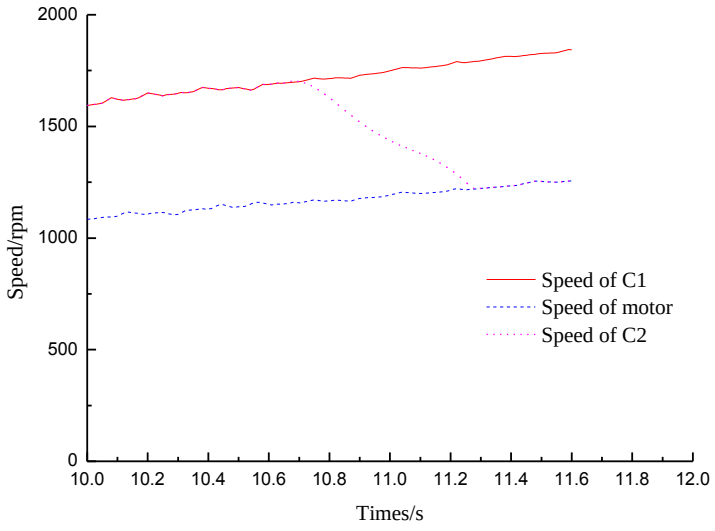

a. Speed of Motor and Clutch

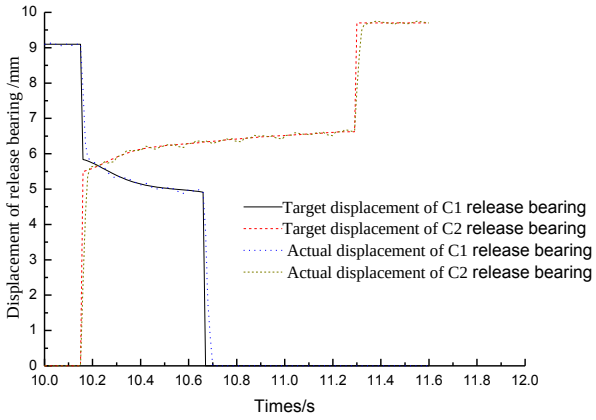

b. Displacement of release bearing

Fig.7. Shifting test results of Electric Vehicle Based on Two-speed DCT

As shown in Figure 7, the vehicle entered the gear shifting process at 10.14s, when the release bearing displacement of the current clutch C1 dropped suddenly, marking the change from the complete engagement to the intermediate state; in the meantime, the release bearing displacement of the target clutch C2 soared, eliminating the empty stroke of the lever spring. Then, the release bearing displacement of clutch C1 declined gradually, while that of clutch C2 gradually increased. In this case, both clutches stayed in the intermediate state. When the torque interaction completed at 10.67s, the release bearing displacement of C1 plunged, signifying the complete separation state, while the that of C2 continued to increase to ensure the complete engagement. At this moment, the entire gear shifting process was wrapped up. Throughout the process, the actual release bearing displacements of the two clutches were tracked accurately and rapidly, which verifies the effectiveness of the proposed control strategy.

Conclusions

(1) To design an ideal two-speed DCT for electric vehicles, this paper constructs the lever spring model of dual dry clutch, torque transmission model of friction plate, and clutch actuator model, paving the way to the analysis of dry clutch displacement-torque features. Then, a proportional flow control valve model was established to analyse current-displacement features of clutch actuator.

(2) The author proposed a clutch displacement servo control strategy based on single-neuron adaptive PID compensation. Through real-time adjustment of the control parameters, the strategy

succeeds in compensating the system nonlinearity and the time-varying features of the control process.

(3) The clutch displacement servo control of the gear shifting process was tested on an electric vehicle installed with a two-speed DCT. The results demonstrate that the proposed strategy can achieve fast and accurate control of the release bearing displacements of the clutches.

Acknowledgement

Supported by Major Program of National Natural Science Foundation of Jiangsu Higher Education Institutions of China (13KJA580001), Natural Science Foundation of Jiangsu Province(BK20150515), Scientific Research Starting Foundation for the senior of Jiangsu university(14JDG155).

References

1. F. Chiara, M.A. Canova, Review of energy consumption, management, and recovery in automotive systems, with considerations of future trends, 2013, Proceedings of the Institution of Mechanical Engineers, Part D: Journal of Automobile Engineering, vol. 227, no. 6, pp. 914-936.
2. I.A. Nienhueser, Y. Qiu, Economic and environmental impacts of providing renewable energy for electric vehicle charging- A choice experiment study, 2016, Applied Energy, vol. 180, pp. 256-268.
3. Z. Rezvani, J. Jansson, J. Bodin, Advances in consumer electric vehicle adoption research: A review and research agenda, 2015, Transportation research part D: Transport and Environment, vol. 34, pp. 218-232.
4. M.S. Kumar, S.T. Revankar, Development scheme and key technology of an electric vehicle: An overview, 2017, Renewable & Sustainable Energy Reviews, vol. 70, pp. 1266-1258.
5. L.D. Novellis, A.S.P. Gruber, Design and comparison of the handling performance of different electric vehicle layouts, 2014, Proceedings of the Institution of Mechanical Engineers, Part D: Journal of Automobile Engineering, vol. 228, no. 2, pp. 218-232.
6. M. Ehsani, Y. Gao, A. Emadi, Modern electric, hybrid electric, and fuel cell vehicles: fundamentals, theory, and design, 2009, CRC Press.
7. D.T. Qin, B.H. Zhou, M.H. Hu, J.J. Hu, X. Wang, Parameters design of powertrain system of electric vehicle with two-speed gearbox, 2011, Journal of Chongqing University, vol. 34, no. 1, pp. 1-6.

8. F.D. Nicola, A. Sorniotti, T. Holdstock, F. Viotto, S. Bertolotto, Optimization of a multiple-speed transmission for downsizing the motor of a fully electric vehicle, 2012, SAE International Journal of Alternative Powertrains, vol. 1, no. 1, pp. 134-143.
9. T. Hofman, C.H. Dai, Energy efficiency analysis and comparison of transmission technologies for an electric vehicle, 2010, IEEE Vehicle Power and Propulsion Conference, Lille, France, pp. 1-6.
10. Q. Ren, D.A. Crolla, A. Morris, Effect of transmission design on electric vehicle (EV) performance, 2009, IEEE Vehicle Power and Propulsion Conference, Michigan, USA, pp. 1260-1265.
11. Z. Jing, C. Fu, N. Gan, Matching Design and Simulation of Electric Vehicle's Powertrain, 2013, Chinese Journal of Automotive Engineering, vol. 3, no. 1, pp. 54-58.
12. A. Sorniotti, S. Subramanyan, A. Turner, C. Cavallino, F. Viotto, Selection of the optimal gearbox layout for an electric vehicle, 2011, SAE International Journal of Commercial Vehicles, vol. 4, no. 1, pp. 1267-1280.
13. X. Zhou, Study of drag torque in a two-speed dual clutch transmission electric vehicle powertrain system, 2014, Sydney: University of Technology Sydney.
14. Y. Wang, E. Lü, H. Lu, N. Zhang, X. Zhou, Comprehensive design and optimization of an electric vehicle powertrain equipped with a two-speed dual-clutch transmission, 2017, Advances in Mechanical Engineering, vol. 9, no. 1, pp. 1-13.
15. S. Hong, H. Son, S. Lee, J. Park, K. Kim, Shift control of a dry-type two-speed dual-clutch transmission for an electric vehicle, 2016, Proceedings of the Institution of Mechanical Engineers, Part D: Journal of Automobile Engineering, vol. 230, no. 3, pp. 308-321.
16. B. Zhu, N. Zhang, P. Walker, W. Zhan, X. Zhou, Two-speed DCT electric powertrain shifting control and rig testing, 2013, Advances in Mechanical Engineering, vol. 2013, pp. 1-10.